SUPPORTING INFORMATION

An unusual mechanism of building up of high magnetization blocking barrier in an octahedral alkoxide Dy^{3+}-based Single-Molecule Magnet

Jérôme Long,*[a] Aleksei O. Tolpygin,[b,c] Ekaterina Mamontova,[a] Konstantin A. Lyssenko,[c,d] Dan Liu,[e] Munirah D. Albaqami,[f] Liviu F. Chibotaru,*[g] Yannick Guari,[a] Joulia Larionova,[a] and Alexander A. Trifonov*[b,c]

[a]*Institut Charles Gerhardt, Equipe Ingénierie Moléculaire et Nano-Objets, Université de Montpellier, ENSCM, CNRS. Place Eugène Bataillon, 34095 Montpellier Cedex 5, France*

[b] *Institute of Organometallic Chemistry of Russian Academy of Sciences, 49 Tropinina str., GSP-445, 630950, Nizhny Novgorod, Russia. E-mail: trif@iomc.ras.ru*

[c]*Institute of Organoelement Compounds of Russian Academy of Sciences, 28 Vavilova str., 119334, Moscow, Russia.*

[d] *Lomonosov Moscow State Univ, Dept. Chem, Leninskie Gory 1, Build 3, Moscow 119991, Russia.*

[e] *Institute of Flexible Electronics (IFE), Northwestern Polytechnical University (NPU), 127 West Youyi Road, Xi'an, 710072, Shaanxi, China.*

[f] *Chemistry Department, College of Science, King Saud University, P.O. Box 2455, Riyadh 11451, Saudi Arabia.*

[g] *Theory of Nanomaterials Group, Katholieke Universiteit Leuven,Celesijnenlaan, 200F, Heverlee, B-3001, Belgium.*

Table of Contents

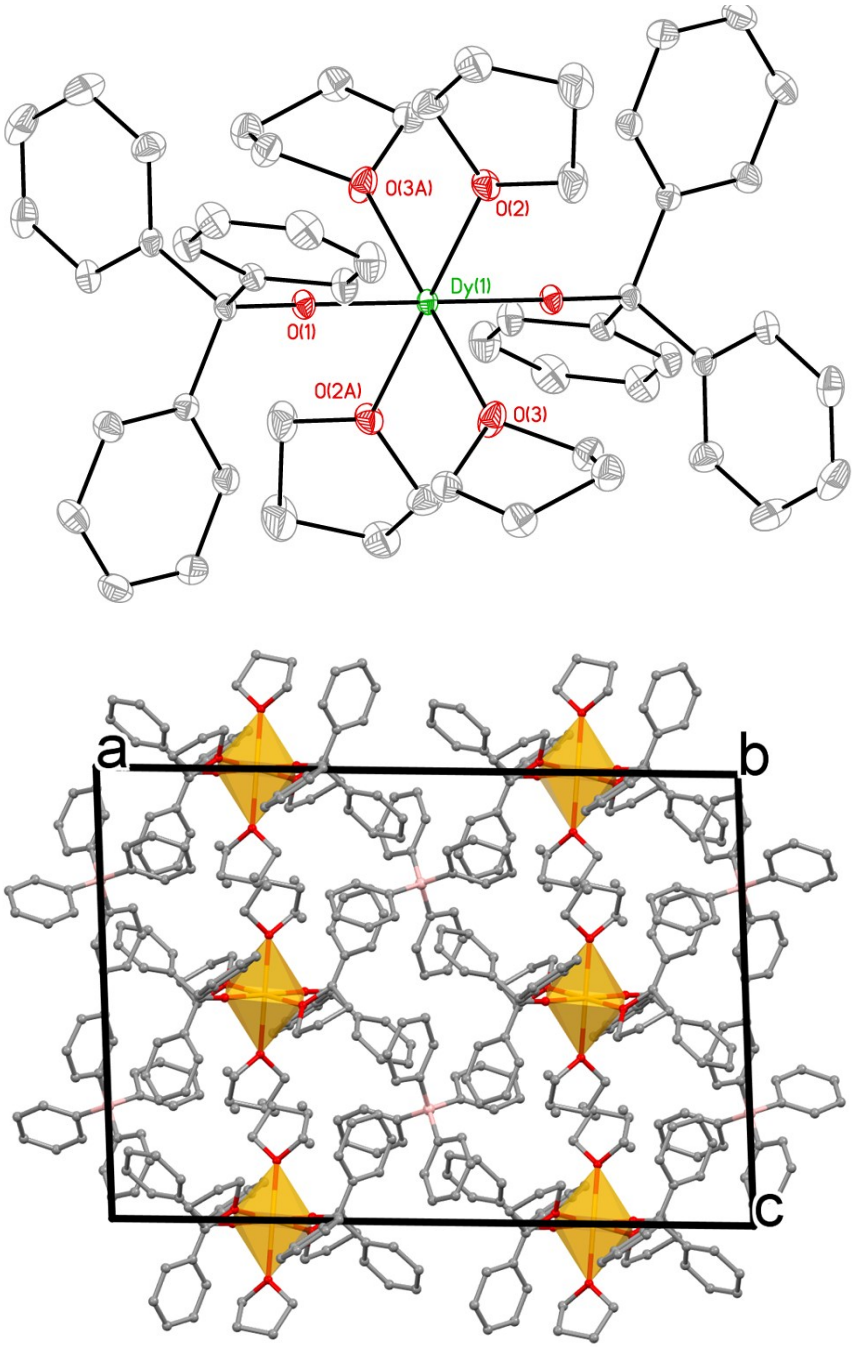

Figure S1: Top: the general view of cation in **1** in representation of atoms by thermal ellipsoids (p=50%). Bottom: perspective views of the crystal packing for **1**. Hydrogen atoms have been omitted for clarity.

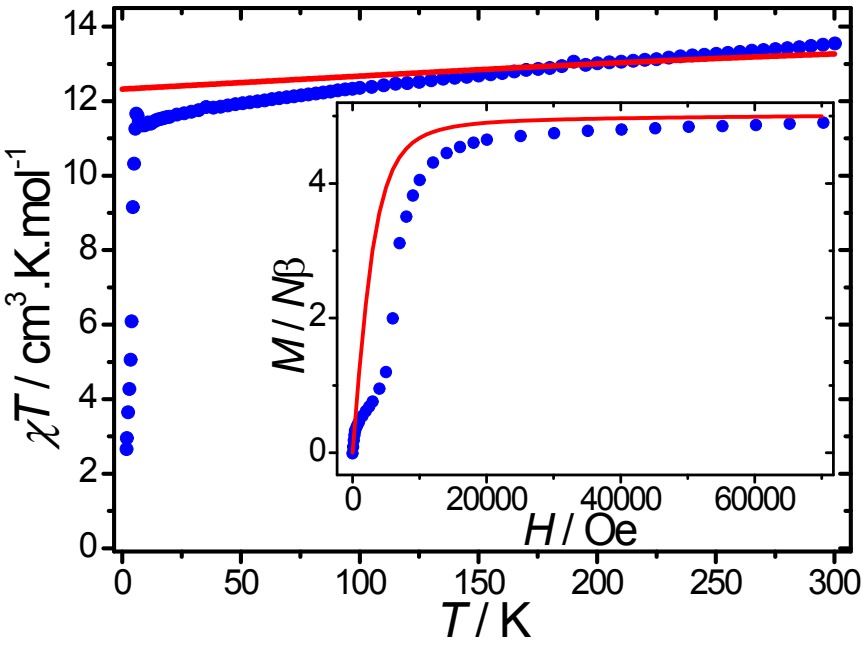

Figure S2: Temperature dependence of χT under an applied magnetic field of 1000 Oe for **1.** The red solid line corresponds to the calculated curve obtained by *ab initio* calculations (CASTP2, full structure). Inset: Field dependence of the magnetization at 1.8 K. The red solid line corresponds to the calculated curves obtained by *ab initio* calculations.

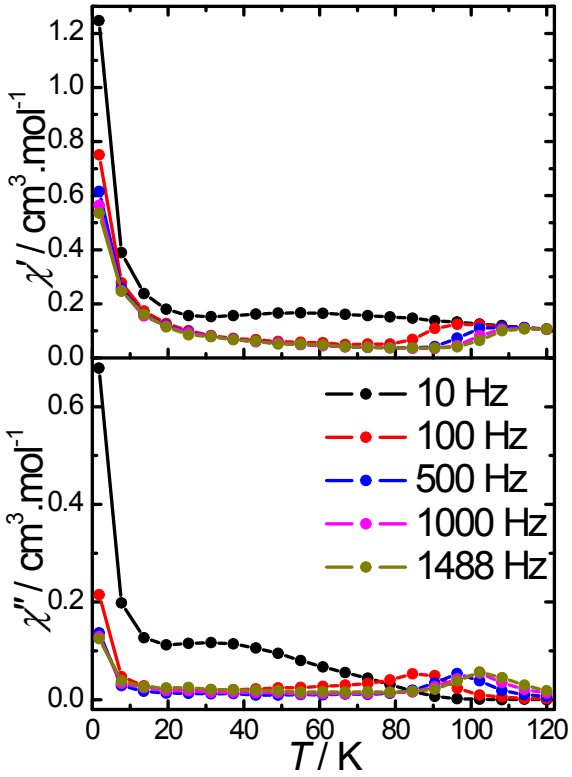

Figure S3. Temperature dependence of χ' and χ'' under a zero dc-field for **1.**

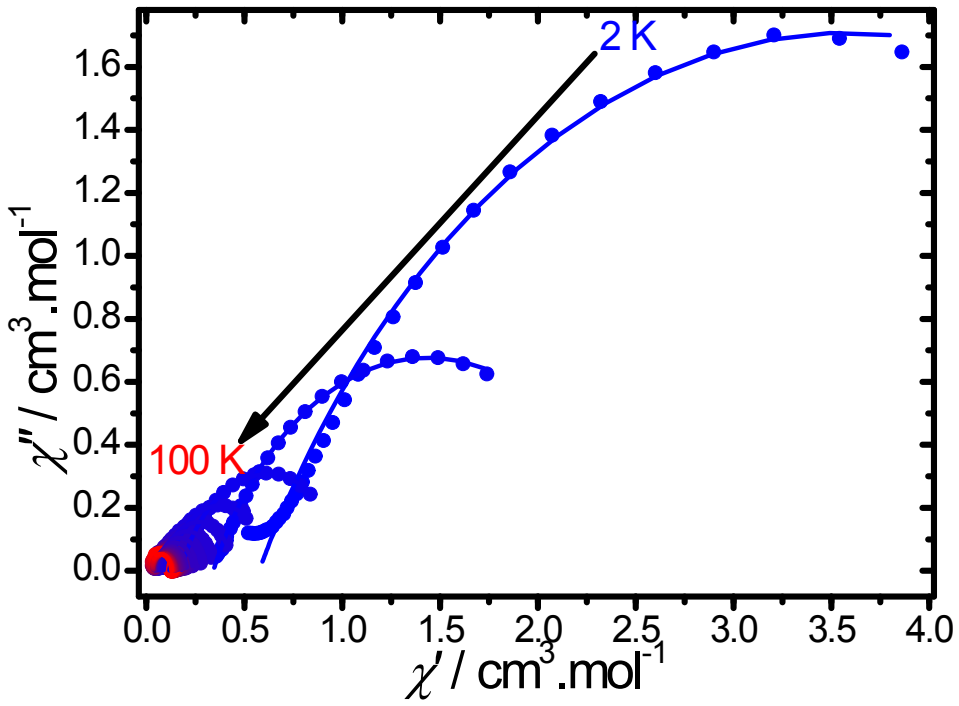

Figure S4: Cole-Cole (Argand) plot obtained using the ac susceptibility data for **1** under a zero dc-field. The solid lines correspond to the best fit obtained with a generalized Debye model.

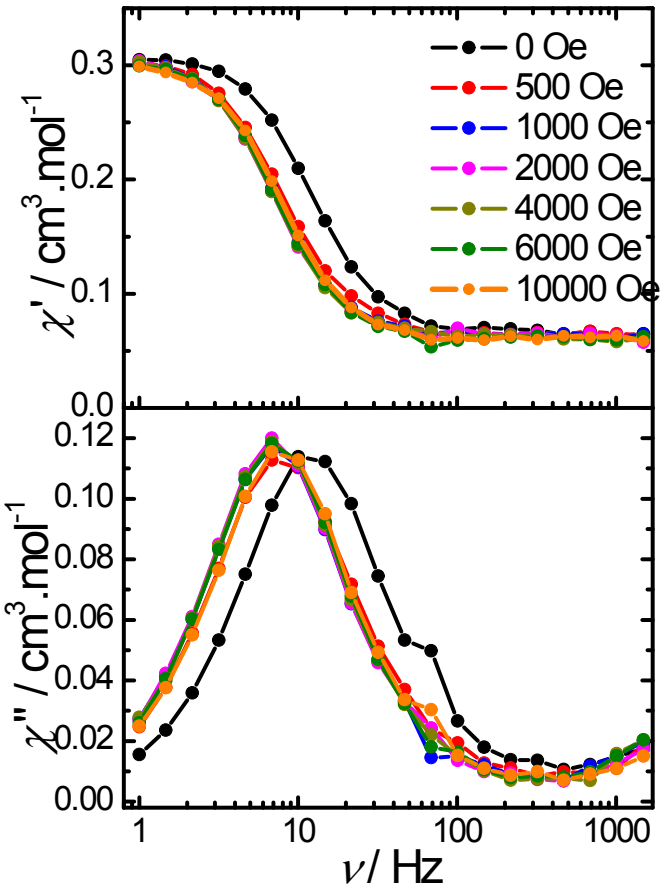

Figure S5. Frequency dependence of χ' and χ'' for compounds **1** (40 K) for various dc fields**.**

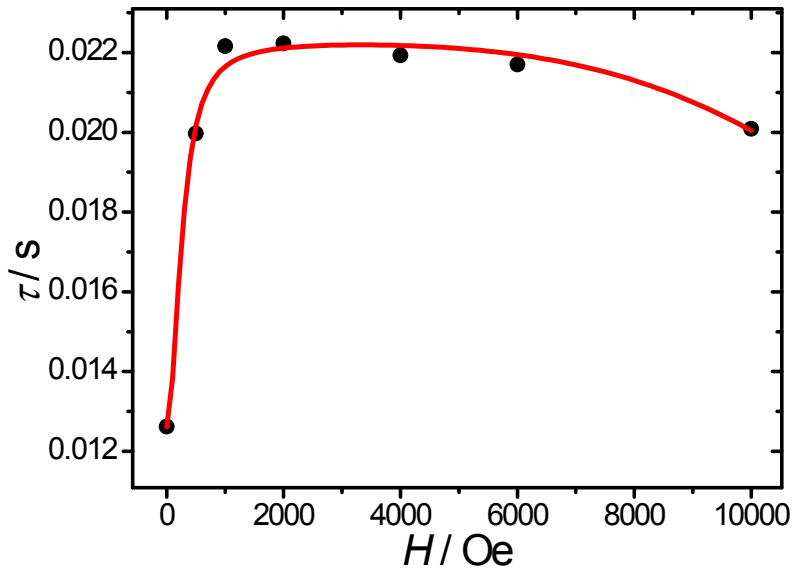

Figure S6. Field dependence of the relaxation time for **1** (40 K). The solid line represents the fit with Equation 2 : $\tau^{-1} = DH^4T + B_1/(1+B_2H^2) + K$ (Eq. 2).

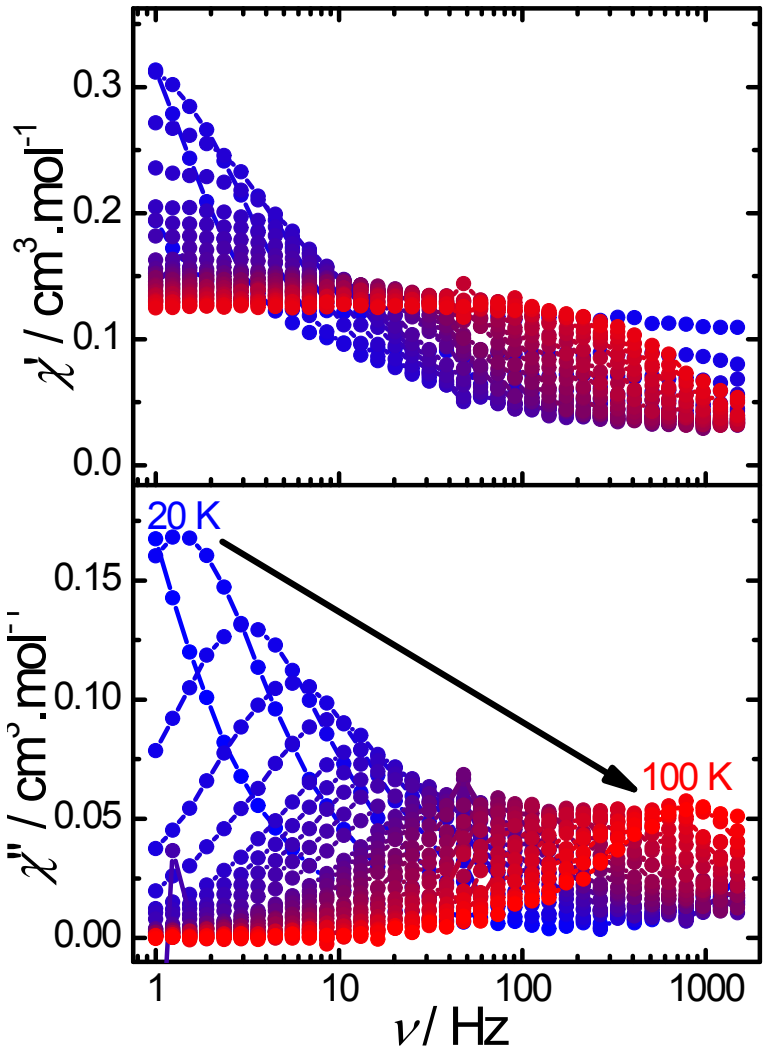

Figure S7. Frequency dependence of χ' and χ'' under a 1000 Oe dc-field for **1**.

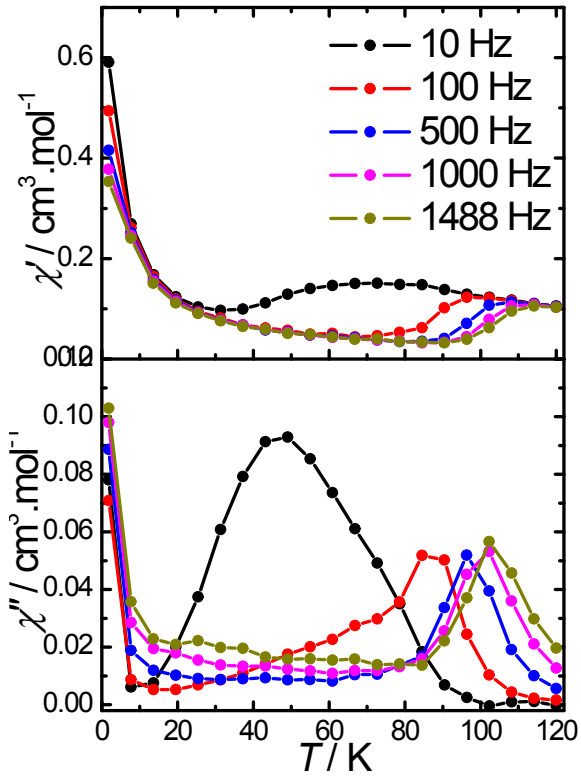

Figure S8: Temperature dependence χ' and χ'' under a 1000 Oe dc-field for **1**.

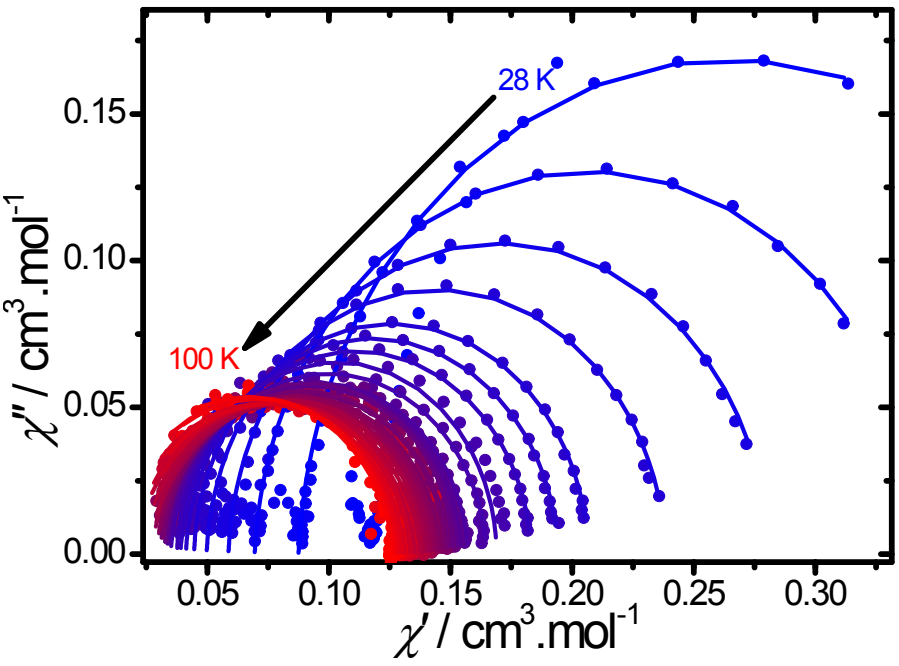

Figure S9: Cole-Cole (Argand) plot obtained using the ac susceptibility data for **1** under a 1000 Oe dc field. The solid lines correspond to the best fit obtained with a generalized Debye model.

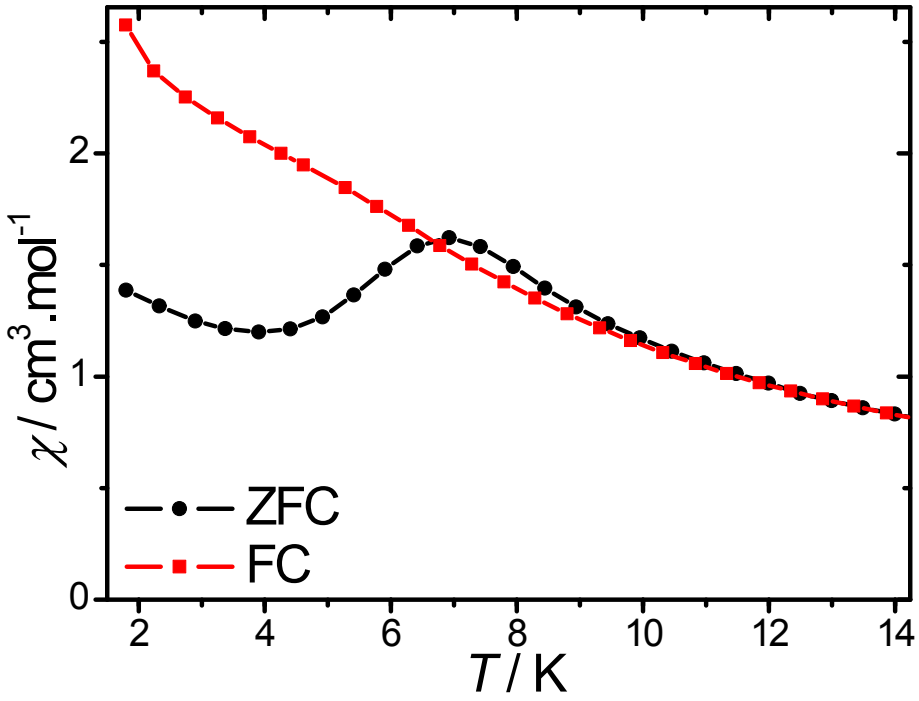

Figure S10: Zero-field cooled (ZFC) and field cooled (FC) curves for **1** obtained under a 2000 Oe dc field.

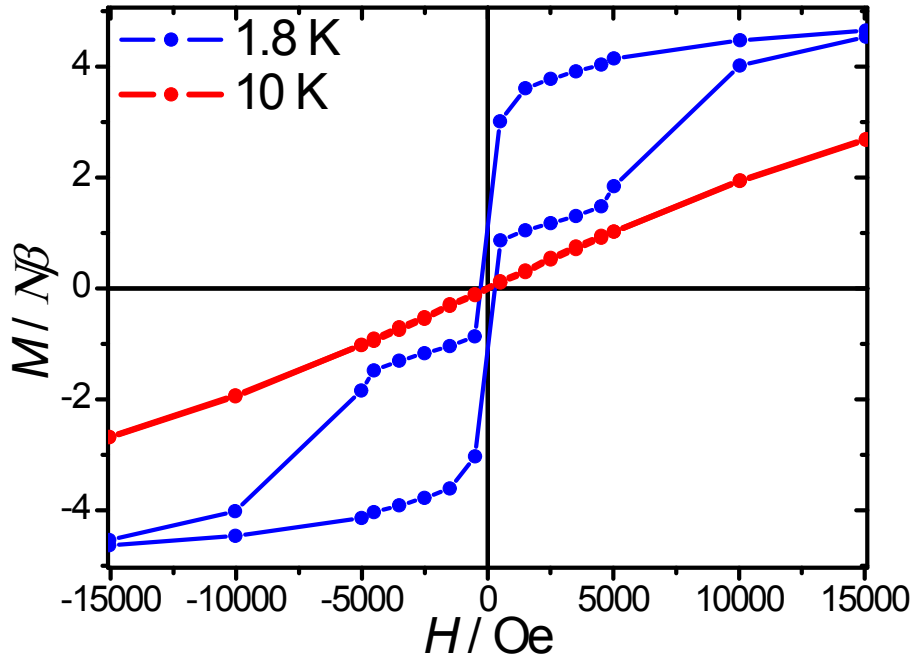

Figure S11: Hysteresis loops for **1** at an average sweep rate of 19 Oe.s^{-1} in the –5000-5000 Oe interval.

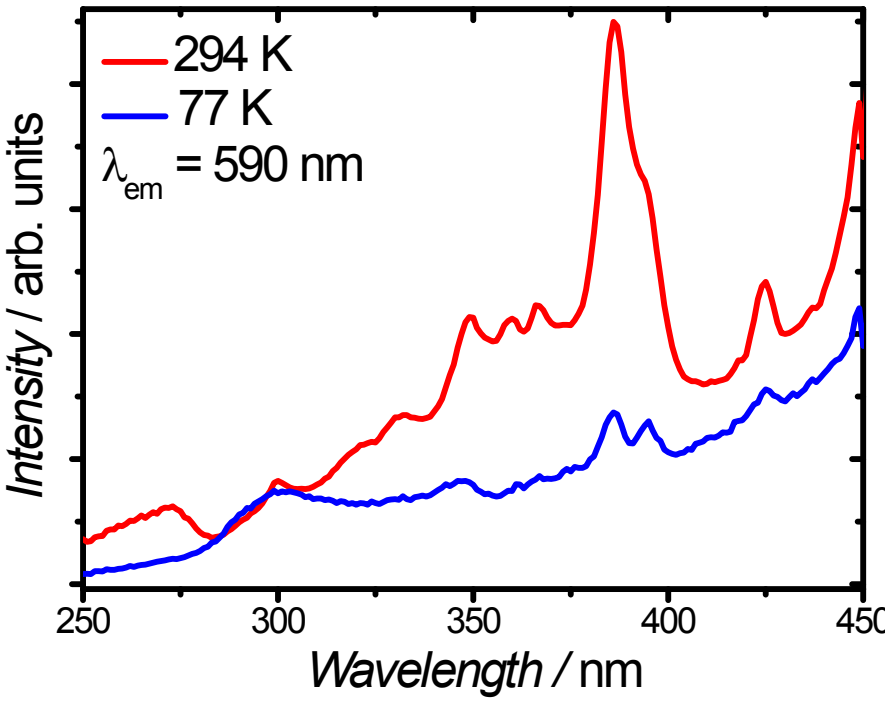

Figure S12. Room and low temperature (77 K) solid-state excitation spectra for **1** monitored at en emission wavelength of 590 nm**.**

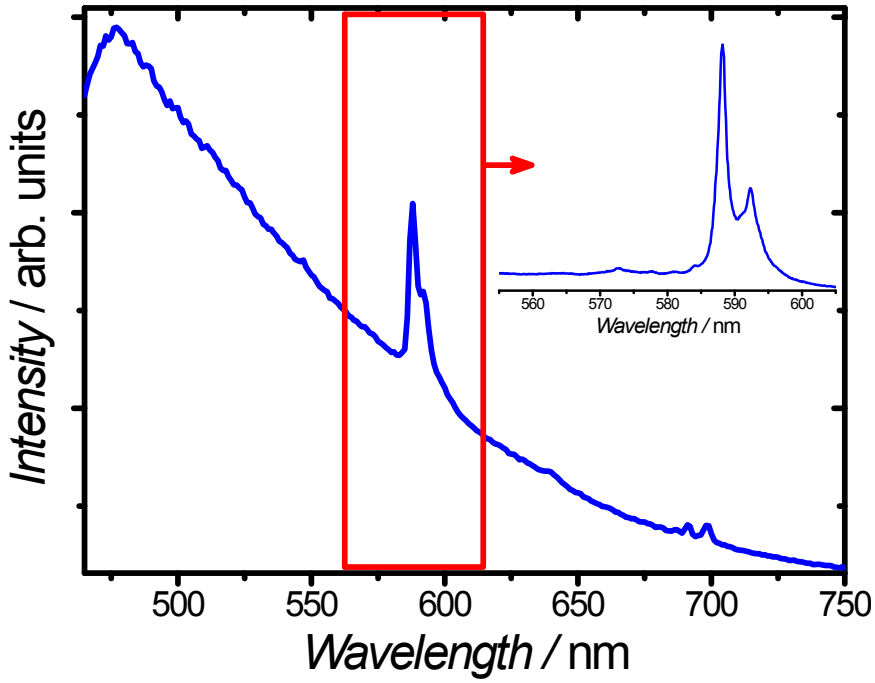

Figure S13. Low temperature (77 K) solid-state emission spectra of **1** acquired at with an excitation wavelength of 387 nm**.**

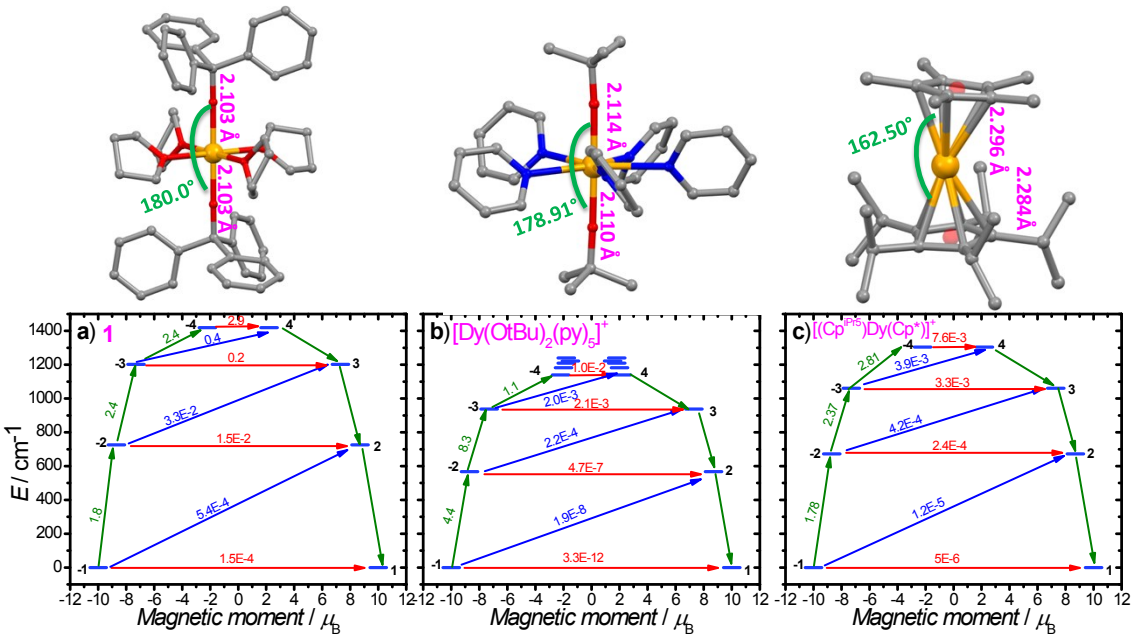

Figure S14. Comparison of the structures and energy diagrams for **1**, $[Dy(O^{tBu})_2(py)_5][BPh_4]$[1] and $[(Cp^{iPr5})Dy(Cp^*)][B(C_6F_5)_4]$.[2] Only the four first excited states are shown for **1** and $[(Cp^{iPr5})Dy(Cp^*)][B(C_6F_5)_4]$. The energy diagrams for $[Dy(O^{tBu})_2(py)_5][BPh_4]$ and $[(Cp^{iPr5})Dy(Cp^*)][B(C_6F_5)_4]$ have been plotted from the data reported in the corresponding publications.[1-2]

Table S1. Crystal data and structure refinement parameters.

	1
CCDC	1943271
Empirical formula	$C_{78}H_{82}BDyO_6$
Formula weight	1288.74
Temperature (K)	120
Crystal system	Monoclinic
Space group	C2/c
Z(Z')	4(0.5)
a, Å	25.613(3)
b, Å	13.7071(11)
c, Å	17.8695(14)
a, °	90
b, °	92.698(3)
g, °	90
V, Å^3	6266.6(9
d_{calc}, g.cm^{-3}	1.366
m, cm^{-1}	12.48
F(000)	2676
$2q_{max}$, °	67.2
Refl. collected	38310
Refl. unique (R_{int})	11640 (0.0282)
Refl. with I > 2σ(I)	9438
Variables	402
Final R_1 with I>2σ(I)	0.0256
wR_2 (all data)	0.0576
GOF	1.036
d_{calc}, g.cm^{-3}	0.524/-0.604

Table S2. SHAPE analysis for compound **1.**

	HP	PPY	OC	TPR	JPPY
1	33.286	29.340	0.337	16.930	35.152

HP: Hexagon
PPY: Pentagonal Pyramid
OC: Octahedron
TPR: Trigonal Prism
JPPY: Johnson Pentagonal Pyramid

Table S3. Key structural parameters in some pentagonal bipyramidal $[Dy(OR)_2(L_{eq})_5]^+$ alkoxide SMMs:

Formula	**Dy-O⁻ Bond lengths**	**O-Dy-O angles °**	**Ref.**
$[Dy(OCPh_3)_2(THF)_4][BPh_4]$ **(1)**	2.103(1)	180°	**This work**
$[Dy(O^tBu)_2(py)_5][BPh_4]$	2.110(2)/ 2.114(2)	178.91(9)	[1] [3]
$[Dy(OPh)_2(THF)_5][BPh_4]$	2.123(3)/ 2.131(3)	176.34(10)	[3]
$[Dy(OPh)_2(py)_5][BPh_4]$	2.1226(40) 2.1222(41)	176.4(3) 176.9(3)	[3]
$[Dy(OCH_2Ph)_2(py)_5][BPh_4]$	2.109(3)/ 2.110(2) 2.089(4)/ 2.116(4)	173.71(17) 179.49(5)	[4]

Table S4. Fitting of the Cole-Cole plots with a generalized Debye model under a zero dc field for **1.**

T (K)	χ_S (cm^3. mol^{-1})	χ_T (cm^3. mol^{-1})	α
5	0.342	2.53	0.295
12	0.177	1.06	0.227
20	0.117	0.64	0.145
28	0.0871	0.446	0.0886
36	0.0706	0.342	0.0481
44	0.0585	0.281	0.0363
52	0.0518	0.238	0.0288
60	0.0444	0.207	0.0222
62.5	0.0443	0.199	0.0183
65	0.0416	0.193	0.0347
67.5	0.0411	0.186	0.0335
70	0.0395	0.179	0.03
72.5	0.0382	0.174	0.0343
75	0.0369	0.168	0.0214
77.5	0.0349	0.163	0.0415
80	0.0346	0.158	0.0305
81	0.0345	0.156	0.0334
82	0.0339	0.154	0.0392
83	0.0327	0.153	0.043
84	0.0331	0.151	0.0355
85	0.0316	0.15	0.0357
86	0.0307	0.147	0.0452
87	0.0305	0.146	0.0386
88	0.0295	0.144	0.0284
89	0.0295	0.143	0.042
90	0.0296	0.142	0.0413
91	0.0268	0.14	0.0487
92	0.0254	0.138	0.0541
93	0.0249	0.137	0.0524
94	0.0234	0.135	0.0521
95	0.0222	0.134	0.0551
96	0.0223	0.132	0.0448
97	0.0215	0.131	0.0277
98	0.0193	0.13	0.0327
99	0.0193	0.13	0.0327
100	0.00963	0.128	0.063

Table S5. Fit parameters of the field dependence of the relaxation time obtained using the Eq. 3; $\tau^{-1} = DH^4T + B_1/(1+B_2H^2) + K$ (Eq. 3), for which the first term accounts for the direct process (for Kramers-ion), the second one stands for the QTM, while the K constant accounts for the field-independent Raman and thermally activated processes.

Compound	D ($s^{-1}K^{-1}Oe^{-4}$)	B_1 (s^{-1})	B_2 (Oe^{-2})	K
1 (40 K)	1.2×10^{-17}	34.4	2.51×10^{-5}	44.9

Table S6. Fitting of the Cole-Cole plots with a generalized Debye model under a 1000 Oe dc field for **1.**

T (K)	χ_S ($cm^3. mol^{-1}$)	χ_T ($cm^3. mol^{-1}$)	α
28	0.0875	0.443	0.0334
36	0.0695	0.344	0.0322
44	0.0587	0.281	0.0309
52	0.0497	0.239	0.0295
60	0.0446	0.207	0.0199
64	0.0412	0.194	0.0247
68	0.039	0.183	0.0263
72	0.0377	0.169	0.00187
76	0.0349	0.165	0.0341
80	0.0339	0.157	0.0355
81	0.0334	0.154	0.0205
82	0.0323	0.153	0.0339
83	0.0327	0.151	0.0102
84	0.0305	0.15	0.053
85	0.0312	0.148	0.0304
86	0.0291	0.146	0.0527
87	0.0293	0.145	0.0411
88	0.0274	0.143	0.052
89	0.0271	0.142	0.0562
90	0.0269	0.14	0.0587
91	0.0268	0.139	0.0396
92	0.0239	0.138	0.0629
93	0.0211	0.136	0.0657
94	0.0198	0.134	0.064
95	0.0213	0.134	0.0565
96	0.016	0.131	0.0716
97	0.019	0.13	0.0522
98	0.0123	0.129	0.0585
99	0.0141	0.127	0.0403
100	0.0078	0.127	0.0655

Computational details

CASSCF/RASSI&CASPT2/RASSI for the reduced structure

All calculations were carried out with MOLCAS 8.3.[5] The employed structure of $[Dy(OCPh_3)_2(THF)_4][BPh_4]$ is shown in Figure S14.

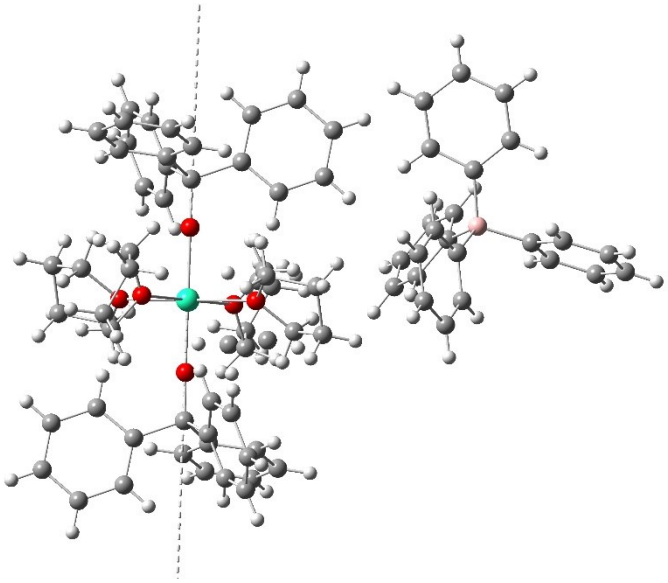

Figure S15. Structure of the Dy complex and the main axiality of ground KD state.

Table S7. Contractions of the employed basis set.

Basis set
DY.ANO-RCC...8S7P5D3F2G1H
B.ANO-RCC...3S2P
O.ANO-RCC...3S2P
C.ANO-RCC...3S2P
H.ANO-RCC...2S

Active space of the CASSCF method included 9 electrons in 7 orbitals for Dy (4*f* orbitals of Dy^{3+} ion). On the basis of the resulting spin-orbital multiplets SINGLE_ANISO module[6] computed local magnetic properties (*g*-tensors, magnetic axes, local magnetic susceptibility, magnetization blocking barrier etc.)

Table S8. Energies and compositionof KDs for the full structure in the CASSCF approximation.

KD	Spin-orbit energies, cm^{-1}	Crystal field Wavefunction
1	0.000	$99.8\%\left\|\pm\frac{15}{2}\right\rangle$
2	557.877	$98.4\%\left\|\pm\frac{13}{2}\right\rangle$
3	930.498	$88.3\%\left\|\pm\frac{11}{2}\right\rangle$
4	1084.375	$33.7\%\left\|\pm\frac{9}{2}\right\rangle+46.1\%\left\|\pm\frac{1}{2}\right\rangle$
5	1193.179	$37.9\%\left\|\pm\frac{9}{2}\right\rangle+12.5\%\left\|\pm\frac{7}{2}\right\rangle+29.5\%\left\|\pm\frac{3}{2}\right\rangle$
6	1231.856	$31.9\%\left\|\pm\frac{7}{2}\right\rangle+36.4\%\left\|\pm\frac{5}{2}\right\rangle+16.7\%\left\|\pm\frac{3}{2}\right\rangle$
7	1318.591	$15.9\%\left\|\pm\frac{9}{2}\right\rangle+10.1\%\left\|\pm\frac{7}{2}\right\rangle+16.2\%\left\|\pm\frac{5}{2}\right\rangle+26.8\%\left\|\pm\frac{3}{2}\right\rangle+27\%\left\|\pm\frac{1}{2}\right\rangle$
8	1348.512	$37.3\%\left\|\pm\frac{7}{2}\right\rangle+31.1\%\left\|\pm\frac{5}{2}\right\rangle+13.2\%\left\|\pm\frac{3}{2}\right\rangle+11.9\%\left\|\pm\frac{1}{2}\right\rangle$

Table S9. *g* tensors of low-lying KD for the full structure in the CASSCF approximation.

KD		CASSCF g
1	g_X	0.000
	g_Y	0.000
	g_Z	19.866
2	g_X	0.048
	g_Y	0.051
	g_Z	16.820
3	g_X	0.350
	g_Y	0.746
	g_Z	13.213
4	g_X	4.104
	g_Y	6.066
	g_Z	11.470
5	g_X	2.195
	g_Y	2.996
	g_Z	9.795
6	g_X	0.852
	g_Y	5.471
	g_Z	13.654
7	g_X	0.074
	g_Y	3.268
	g_Z	14.470
8	g_X	0.386
	g_Y	3.221
	g_Z	15.823

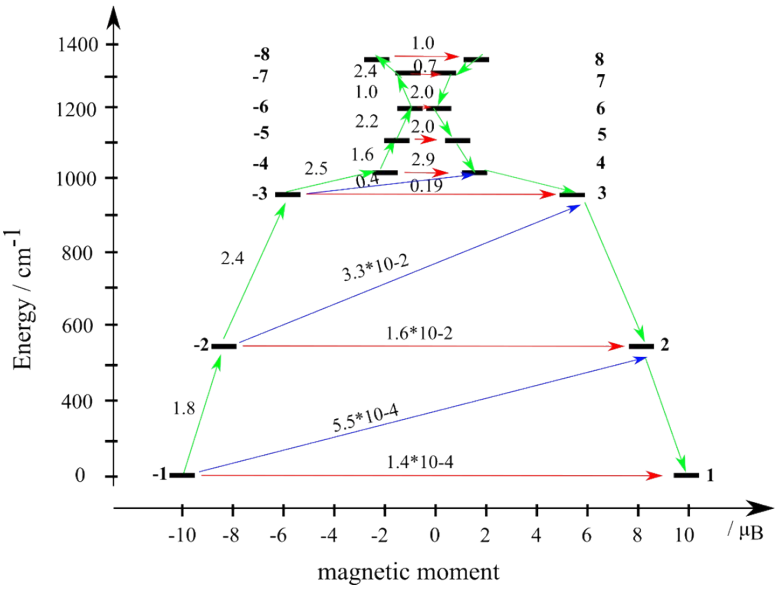

Figure S16. The states are placed on the diagram according to their magnetic moments (bold black lines). The horizontal red lines show the tunneling transitions (the energy splitting) within each doublet state, while the nonhorizontal lines show the spin-phonon transition paths. The numbers at non-horizontal lines are averaged transition moments in μB connecting the corresponding states. The numbers at horizontal lines are tunneling gaps. The green arrows delineate the relaxation path.

CASSCF/RASSI & CASPT2/RASSI for the reduced structure

Because the experimental structure is too large for a CASPT2 treatment, we employed a recently proposed methodology[7] to evaluate the CASPT2 correction to the crystal field (CF) based on the calculations of a reduced fragment of the structure. The idea is to extract the CF parameters from CASSCF/RASSI and CASPT2/RASSI calculations for a core of the structure (reduced structure). Then the correction due to dynamical correlation is simply the difference of the corresponding CF parameters. The latter is added to the CF parameters derived from CASSCF/RASSI of the full (experimental) structure described in the previous section. The extraction of CF parameters at each calculations is done routinely with the SINGLE_ANISO module of MOLCAS package.[6]

The experimental structure of was cut to a fragment where the $B(C_6H_5)_4$ was omitted and $C(C_6H_5)_3$ and C_4H_8O groups have been replaced with CH_3 and H_2O groups, respectively (Figure S16).

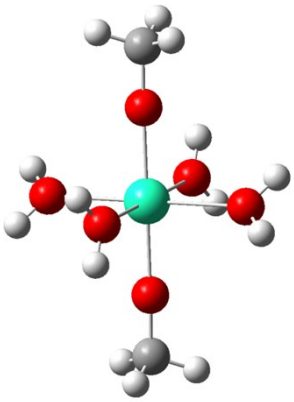

Figure S17. The reduced structure.

Table S10. Contractions of the employed basis set.

Basis set
DY.ANO-RCC...7S6P4D2F1G.
O.ANO-RCC...3S2P
C.ANO-RCC...3S2P
H.ANO-RCC...2S

Table S11. Energies and composition of low-lying KD for the reduced structure.

KD	Spin-orbit energies, cm^{-1}	Crystal field Wavefunction	Spin-orbit energies, cm^{-1}	Wavefunctions' composition
	CASSCF	CASSCF	CASPT2	CASPT2
1	0.000	$99.9\%\left\|\pm\frac{15}{2}\right\rangle$	0.000	$99.9\%\left\|\pm\frac{15}{2}\right\rangle$
2	630.812	$99.3\%\left\|\pm\frac{13}{2}\right\rangle$	797.239	$99.7\%\left\|\pm\frac{13}{2}\right\rangle$
3	1098.491	$96\%\left\|\pm\frac{11}{2}\right\rangle$	1362.508	$98.4\%\left\|\pm\frac{11}{2}\right\rangle$
4	1375.834	$74.5\%\left\|\pm\frac{9}{2}\right\rangle+16.6\%\left\|\pm\frac{1}{2}\right\rangle$	1691.935	$89.6\%\left\|\pm\frac{9}{2}\right\rangle$
5	1488.473	$12.9\%\left\|\pm\frac{9}{2}\right\rangle+31\%\left\|\pm\frac{7}{2}\right\rangle+19.4\%\left\|\pm\frac{3}{2}\right\rangle+25.5\%\left\|\pm\frac{1}{2}\right\rangle$	1792.499	$27.8\%\left\|\pm\frac{7}{2}\right\rangle+10.8\%\left\|\pm\frac{5}{2}\right\rangle+23.5\%\left\|\pm\frac{3}{2}\right\rangle+35.7\%\left\|\pm\frac{1}{2}\right\rangle$
6	1552.088	$27\%\left\|\pm\frac{7}{2}\right\rangle+38.2\%\left\|\pm\frac{5}{2}\right\rangle+27.1\%\left\|\pm\frac{3}{2}\right\rangle$	1865.566	$40.4\%\left\|\pm\frac{7}{2}\right\rangle+30.1\%\left\|\pm\frac{5}{2}\right\rangle+20.4\%\left\|\pm\frac{3}{2}\right\rangle$
7	1622.774	$16.4\%\left\|\pm\frac{7}{2}\right\rangle+11\%\left\|\pm\frac{5}{2}\right\rangle+23.6\%\left\|\pm\frac{3}{2}\right\rangle+40.4\%\left\|\pm\frac{1}{2}\right\rangle$	1935.130	$13.9\%\left\|\pm\frac{7}{2}\right\rangle+10.8\%\left\|\pm\frac{5}{2}\right\rangle+23.3\%\left\|\pm\frac{3}{2}\right\rangle+47.8\%\left\|\pm\frac{1}{2}\right\rangle$
8	1667.206	$18.9\%\left\|\pm\frac{7}{2}\right\rangle+37.9\%\left\|\pm\frac{5}{2}\right\rangle+25.6\%\left\|\pm\frac{3}{2}\right\rangle+14.6\%\left\|\pm\frac{1}{2}\right\rangle$	1977.414	$15.5\%\left\|\pm\frac{7}{2}\right\rangle+44.7\%\left\|\pm\frac{5}{2}\right\rangle+30.7\%\left\|\pm\frac{3}{2}\right\rangle$

Table S12. The *g* tensors of the lowest KDs for the reduced structure.

KD		CASSCF g	CASPT2 g
1	g_X	0.000	0.000
	g_Y	0.000	0.001
	g_Z	19.876	19.869
2	g_X	0.012	0.009
	g_Y	0.013	0.011
	g_Z	16.866	16.793
3	g_X	0.058	0.075
	g_Y	0.090	0.092
	g_Z	13.914	13.996
4	g_X	3.269	1.208
	g_Y	4.856	1.483
	g_Z	9.316	10.887
5	g_X	9.969	2.174
	g_Y	6.669	3.625
	g_Z	1.696	15.219
6	g_X	1.085	2.489
	g_Y	2.199	3.778
	g_Z	15.262	12.694
7	g_X	0.458	0.425
	g_Y	0.597	0.880
	g_Z	17.792	17.035
8	g_X	0.028	0.2295
	g_Y	0.475	0.809
	g_Z	18.326	17.613

Table S13. Calculated energies (cm^{-1}) of the eight lowest KDs arising from the crystal field splitting of the $^6H_{15/2}$ manifold

KD	Full structure	Reduced structure		Full structure (CASPT2 corrected CF)[b]
	CASSCF	CASSCF	CASPT2	
1	0.000	0.000	0.000	0.000
2	557.877	630.812	797.239	725.654
3	930.498	1098.491	1362.508	1202.049
4	1084.375	1375.834	1691.935	1419.717
5	1193.179	1488.473	1792.499	1480.346
6	1231.856	1552.088	1865.566	1536.032
7	1318.591	1622.774	1935.130	1594.644
8	1348.512	1667.206	1977.414	1691.693

[b] Calculated by diagonalizing a CF Hamiltonian obtained as a sum of the CF from a CASSCF calculation on the full structure and a correction due to dynamic electron correlation obtained as a difference of CF from a CASSCF and a CASPT2 calculation for the reduced structure.[3]

CASSCF/RASSI & CASPT2/RASSI calculations for the a structure with elongated equatorial Dy-O bonds

In order to investigate the effect of weakening of the equatorial crystal field on the blocking properties of complex, its geometry has been modified with respect to the experimental one (Figure S15) by elongating the four equatorial Dy-O bonds by 0.1 Å. The CASSCF/RASSI & CASPT2/RASSI calculations have been done in the similar way to the original structure (see above). The resulting blocking barrier is shown in Fig. 18.

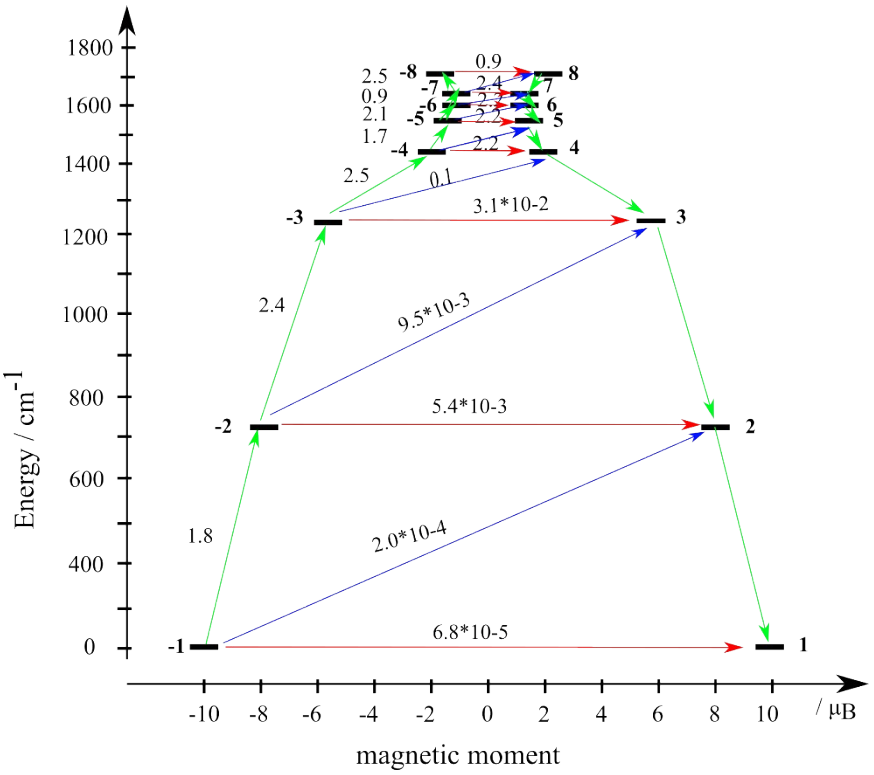

Figure S18. The same as in Figure 16 for a geometry modified by elongating the four Dy-O bonds in the equatorial plane**.**

References

[1] Y.-S. Ding, N. F. Chilton, R. E. P. Winpenny, Y.-Z. Zheng, *Angew. Chem. Int. Edit.* **2016**, *55*, 16071-16074.

[2] F.-S. Guo, B. M. Day, Y.-C. Chen, M.-L. Tong, A. Mansikkamäki, R. A. Layfield, *Science* **2018**, *362*, 1400-1403.

[3] Y. S. Ding, T. Han, Y. Q. Zhai, D. Reta, N. F. Chilton, R. E. P. Winpenny, Y. Z. Zheng, *Chem. Eur. J.* **2020**, *26*, 5893-5902.

[4] K.-X. Yu, J. G. Kragskow, Y.-S. Ding, Y.-Q. Zhai, D. Reta, N. F. Chilton, Y.-Z. Zheng, *Chem* **2020**, *6*, 1777-1793.

[5] F. Aquilante, J. Autschbach, R. K. Carlson, L. F. Chibotaru, M. G. Delcey, L. De Vico, I. Fdez. Galván, N. Ferré, L. M. Frutos, L. Gagliardi, M. Garavelli, A. Giussani, C. E. Hoyer, G. Li Manni, H. Lischka, D. Ma, P. Å. Malmqvist, T. Müller, A. Nenov, M. Olivucci, T. B. Pedersen, D. Peng, F. Plasser, B. Pritchard, M. Reiher, I. Rivalta, I. Schapiro, J. Segarra-Martí, M. Stenrup, D. G. Truhlar, L. Ungur, A. Valentini, S. Vancoillie, V. Veryazov, V. P. Vysotskiy, O. Weingart, F. Zapata, R. Lindh, *J. Comput. Chem.* **2016**, *37*, 506-541.

[6] L. Ungur, L. F. Chibotaru, in *http://www.molcas.org/documentation/manual/*, **2006-2013**.

[7] L. Ungur, L. F. Chibotaru, *Chem. Eur. J.* **2017**, *23*, 3708-3718.